Applied Thermal Engineering 64 (2014) 371–375

Contents lists available at ScienceDirect

Applied Thermal Engineering

journal homepage: www.elsevier.com/locate/apthermeng

Direct molecular diffusion and micro-mixing for rapid dewatering of LiBr solution

Sajjad Bigham, Rasool Nasr Isfahani, Saeed Moghaddam*

Department of Mechanical and Aerospace Engineering, University of Florida, Gainesville, FL 32611, USA

HIGHLIGHTS

- A method for mixing an absorbent film constrained by a porous membrane is introduced.
- The method involves continuous replenishment of the absorbent–vapor interface.
- A desorption rate higher than that of boiling is achieved.

ARTICLE INFO

Article history:
Received 9 October 2013
Accepted 13 December 2013
Available online 28 December 2013

Keywords:
Adsorption refrigeration system
Desorption process
Memrbane-based desorption

ABSTRACT

A slow molecular diffusion rate often limits the desorption process of an absorbate molecule from a liquid absorbent. To enhance the desorption rate, the absorbent is often boiled to increase the liquid–vapor interfacial area. However, the growth of bubbles generated during the nucleate boiling process still remains mass-diffusion limited. Here, it is shown that a desorption rate higher than that of boiling can be achieved, if the vapor–absorbent interface is continuously replenished with the absorbate-rich solution to limit the concentration boundary layer growth. The study is conducted in a LiBr–water solution, in which the water molecules' diffusion rate is quite slow. The manipulation of the vapor–solution interface concentration distribution is enabled by the mechanical confinement of the solution flow within microchannels, using a hydrophobic vapor-venting membrane and the implementation of microstructures on the flow channel's bottom wall. The microstructures stretch and fold the laminar streamlines within the solution film and produce vortices. The vortices continuously replace the concentrated solution at the vapor–solution interface with the water-rich solution brought from the bottom and middle of the flow channel. The physics of the process is described using a combination of experimental and numerical studies.

Published by Elsevier Ltd.

1. Introduction

The desorption process is utilized in many industrial applications, such as absorption refrigeration systems (ARSs). Desorbers involving nucleate pool boiling [1–3] and falling film over horizontal or vertical tubes [4–6] are the common configurations in lithium bromide (LiBr) ARSs. In the pool boiling configuration, as the name implies, water is boiled off from a pool of LiBr solution. In a falling film desorber, the LiBr solution is sprayed over a tube bundle while the heating medium flows inside the tubes. The falling-film type of desorbers are more suitable for ARSs, particularly with low temperature heat sources [7], since the formation of thin solution films over the tubes facilitates water desorption. At low surface temperatures, water directly diffuses out of the solution film, as long as the solution temperature is high enough to sustain a solution water vapor pressure above the external vapor pressure.

When the wall temperature sufficiently exceeds the solution saturation temperature, desorption also begins to take place into bubbles nuclei formed at the solid–liquid interface. Charters et al. [1] and Yoshitomi et al. [8] suggested that a superheat temperature (the difference between the wall and the solution saturation temperature) of approximately 10 °C is required for boiling inception. It is known that the water bubble growth rate is significantly slow [9] because of the low water diffusion coefficient in the LiBr solution. In other words, bubble growth in the LiBr solution is limited by mass diffusion rather than by heat transfer, as in pure water. Consequently, a significant surface superheat temperature is required to grow the bubbles large enough to enable departure from the heat transfer surface (the buoyancy force should overcome the surface tension force for departure).

* Corresponding author.
E-mail address: saeedmog@ufl.edu (S. Moghaddam).

1359-4311/$ – see front matter Published by Elsevier Ltd.
http://dx.doi.org/10.1016/j.applthermaleng.2013.12.031

An increase in the desorption rate and a reduction of the required surface superheat temperature have often been desired for the obvious reasons of reducing the size of a desorber and lowering its required heating medium temperature. The need for the implementation of renewable energy sources for heating/cooling buildings has invigorated efforts to advance the absorption cycles technology. In the use of an absorption cycle with solar-thermal collectors or photovoltaics with waste heat recovery, the reduction of the required heat source temperature benefits the system and enhances the prospect of directly converting solar heat to a cooling effect. However, operation of absorption cycles at high temperatures often reduces the efficiency of solar collectors and limits the applicable collector technologies.

A recently proposed desorber configuration [10–15] has provided an opportunity to achieve the aforementioned objectives. In the new approach, the LiBr solution is mechanically constrained within a desired thickness by a vapor-permeable hydrophobic membrane. The membrane allows the vapor to exit the flow while the liquid is retained. Confinement of the flow provides a level of control over the thermohydraulics of the flow unachievable in a falling film desorber configuration. Experimental studies on thin solution films within microchannels with smooth walls have shown a significant enhancement in desorption rate as compared to the existing falling film technology [12,13]. In this work, further enhancement of the desorption process is sought through utilization of microstructures on the microchannel walls. Such structures have been readily implemented in mixing the laminar flow in microchannels [16–19]. In this case, confinement of the LiBr solution flow has provided an opportunity to similarly manipulate the microscale transport events within the solution film. The objective here is to always move the concentrated solution away from the membrane–solution interface, and carry the water-rich solution from the middle and bottom of the flow channel to the membrane–solution interface.

In the following sections, first, the desorption process from a solution flow confined within microchannels with smooth walls is experimentally studied. The studies are conducted in single and two phase flow regimes. Then, a numerical model is utilized [10,14] to illustrate mass diffusion limitations of the process. Finally, the numerical model is used to study the impact of surface microstructures on the desorption process. It is shown that a desorption rate higher than that of the boiling regime could be achieved.

2. Experiment

A schematic of the desorber heat exchanger is provided in Fig. 1. The overall size of the desorber is 16.8 × 16.5 cm^2. The solution microchannels are machined on a corrosion-resistant C-22 Hastelloy over a 5.7 × 8.9 cm^2 area. A hydrophobic nanofibrous membrane is placed on the solution microchannels and secured in place by a perforated stainless steel sheet. This arrangement forms 200 ± 10 μm thick solution channels (verified by comparing the solution pressure drop with the laminar flow theory). Twelve thermocouples are installed within three trenches machined on the backside of the Hastelloy plate to measure the wall temperature. The remaining space within the trenches is filled with a high temperature conductive epoxy, and a flexible thin-film heater (Omega Engineering, CT) is subsequently assembled over the entire surface.

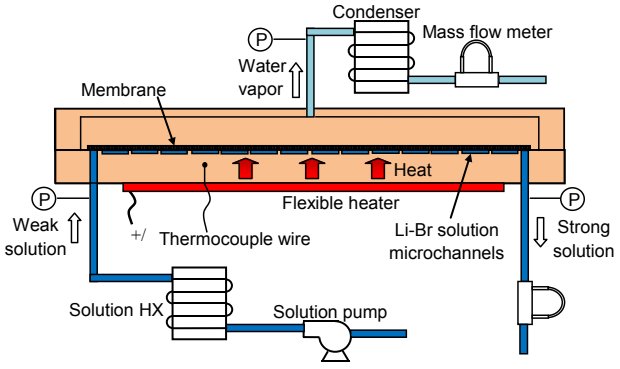

Fig. 1. Schematic diagram of the desorber heat exchanger.

To test the desorber, a micro gear pump (HNP Mikrosysteme, Germany) drives the weak LiBr solution through a solution heat exchanger, where the solution is preheated to the desired temperature before entering the desorber. In the desorber, the weak LiBr solution is heated by the thin-film heater to desorb water. The desorbed water vapor flows to a condenser, and the strong LiBr solution leaves the desorber and enters a Coriolis mass flow meter (Bronkhorst USA), where the LiBr solution flow rate and concentration are evaluated. The condensed water leaves the condenser and flows through a Coriolis mass flow meter (Micro Motion, Inc.), where the desorption rate is directly measured. Three pressure transducers with a range of 0–100 kPa have been installed to monitor desorber pressure conditions. Two of the transducers measure the LiBr solution flow pressure at the desorber inlet and outlet. The average solution pressure (P_s) is calculated using the readings of these transducers. The third transducer measures the vapor pressure (P_v) at the desorber vapor exit. Further details regarding the experimental loop are available in Isfahani and Moghaddam [11]. All tests are conducted at a solution flow rate of 2.5 kg/hr and a solution inlet temperature of 60 °C.

3. Numerical modeling

The numerical domain is a rectangular microchannel with a porous hydrophobic top wall and a heated bottom surface. For a detailed discussion about the solver and the numerical procedure, the readers are referred to our prior publication [10,14]. Here, a brief overview of the modeling approach is provided. The numerical procedure consists of two steps. In the first step, a continuum-based approach is used to model the heat and mass transport inside the solution. The governing equations can be summarized as:

$$\rho u_j u_{i,j} = -p_{,i} + \mu u_{i,jj} \tag{1}$$

$$u_j T_{,j} = \alpha T_{,jj} \tag{2}$$

$$u_j X_{,j} = D X_{,jj} \tag{3}$$

where μ is the dynamic viscosity, α is the thermal diffusivity, and D is the mass diffusivity.

In the second step, to simulate the vapor flux through the membrane, the Dusty-Gas model [20] is used, since the flow is in the transitional or free molecular flow regime [10]. The accuracy of the model has been established in a recent study [12].

$$J = k_m(P_v - P_{s,w}), k_m = -(M/\delta_m)\left[D_e^k/(RT) + PB_0/RT\mu\right] \tag{4}$$

where k_m is the membrane mass transfer coefficient, P_v is the water vapor pressure, and $P_{s,w}$ is the water vapor pressure of the solution at the interface.

At the vapor–solution interface, it is assumed that the water vapor and LiBr solution are in equilibrium [10,14,20,21]:

$$k(T,X)\partial T/\partial n = h_{fg}(T,X)\cdot k_m\left(P_v - P_{s,w}(T,X)\right) \quad (5)$$

$$D(T,X)\rho(T,X)\partial X/\partial n = k_m\left(P_v - P_{s,w}(T,X)\right) \quad (6)$$

The LiBr properties were obtained from Ref. [22]. To solve the governing equations with the mentioned boundary conditions, an in-house computational fluid dynamics solver based on the Lattice Boltzmann Method (LBM) is used [23,24]. A grid independence study was performed. The grid size is 3 μm in all three directions.

4. Results and discussion

4.1. Base Case

As mentioned earlier, first, the desorption process in microchannels without any surface features was experimentally and numerically studied. Fig. 2 shows the experimental desorption rates (all unfilled symbols) as a function of wall temperature. The wall temperature, T_w, is the average reading of the twelve thermocouples imbedded within the heated wall.

The first test was conducted at a vapor pressure (P_v) of 6 kPa (vapor pressure in a typical single-effect ARS is between 5 and 10 kPa, depending on the condenser temperature), a solution pressure (P_s) of 23 kPa, and a solution concentration of 48%. Solution pressure was selected sufficiently higher than the vapor pressure such that both modes of desorption could be realized. As shown, the first non-zero desorption rate was measured at a surface temperature of approximately 60 °C. Desorption at this temperature is due to a positive driving pressure between the solution water vapor pressure ($P_{s,w}$) and the external vapor pressure (i.e. $P_{s,w} - P_v > 0$). Thermodynamic properties of the LiBr solution at the desorber inlet concentration confirm that the solution water vapor pressure exceeds 6 kPa at a solution temperature of 60 °C (cf. Fig. 3). The desorption rate then steadily increases with the wall temperature at a moderate pace, since increasing the solution temperature

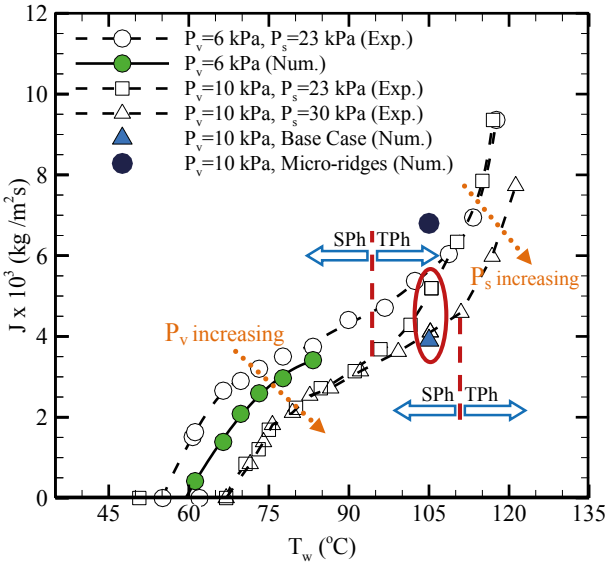

Fig. 2. Variations of the desorption rate versus the wall temperature at different vapor and solution pressures. SPh and TPh stand for single-phase and two-phase desorption modes, respectively. The red dash line marks a significant change in the rate of increase is desorption, suggesting a shift from SPh to TPh desorption mode. (For interpretation of the references to color in this figure legend, the reader is referred to the web version of this article.)

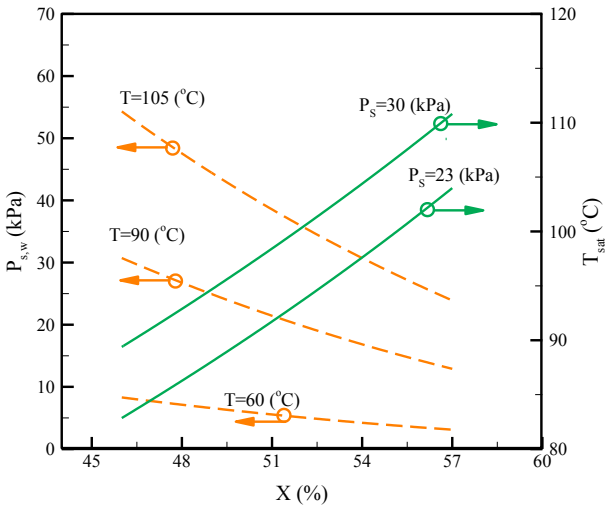

Fig. 3. Solution water vapor pressure ($P_{s,w}$) as a function of temperature and concentration and solution saturation temperature (T_{sat}) as a function of solution pressure and concentration (prepared using Engineering Equation Solver (EES) software, McGraw-Hill).

increases the solution water vapor pressure, and consequently increases the driving pressure potential. The desorption rate diminished when the vapor pressure was increased to 10 kPa, due to reduction of the pressure potential.

Fig. 2 also provides a comparison of the numerical and experimental results. The numerical results (color filled symbols) closely follow the experimental data. The small difference between the two could be mostly due to uncertainty in the film thickness, potential inaccuracy in the solution water vapor pressure correlations used in the numerical code, and non-uniformity of the wall temperature. Also, to understand the cause of the observed decline in the rate of increase in the desorption rate at moderate surface temperatures, a set of numerical simulations was conducted. The results suggested that a small variation in the solution concentration entering the desorber is responsible for the observed behavior. Although efforts were made during the tests to maintain a constant inlet concentration, the system stabilized at a slightly different concentration in each test. This resulted in a gradual increase in the solution inlet concentration from 48% to 51% within a wall temperature range from 60 °C to 83 °C. For a detailed discussion on this subject, readers are referred to Ref. [13].

At the solution pressure of 23 kPa, when the wall temperature was increased a few degrees above the solution saturation temperature (about 93 °C at the average solution concentration of 52%, cf. Fig. 3), the desorption rate started to significantly rise (cf. Fig. 2), signifying a change in the desorption regime. This change was associated with some fluctuations in the desorption rate, solution flow rate, and pressure readings due to instabilities associated with boiling the solution flow. In a subsequent test, the solution pressure was increased to 30 kPa in order to suppress boiling by increasing the solution saturation temperature (to about 103 °C at an average concentration of 53%, cf. Fig. 3), while the other test conditions were kept the same. The test results are compared in Fig. 2, showing a lower desorption rate when boiling is suppressed. Fig. 4 provides a numerical depiction of the LiBr concentration distribution at the solution pressure of 30 kPa (the inlet concentration is 52%). The figure highlights the fact that a significant portion of the solution does not participate in the desorption process due to a slow water molecules diffusion rate. A comparison of the numerical (i.e. "Base Case") and experimental desorption rates are also provided in Fig. 2.

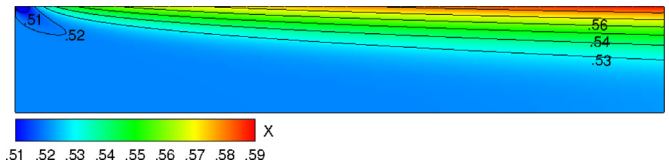

Fig. 4. LiBr solution concentration contours within a 200-μm-thick and 89-mm-long flow channel.

4.2. Implementation of surface-induced vortices

To continuously bring the water-rich solution in contact with the membrane, micro-ridges are designed on the bottom wall of the flow channel (cf. Fig. 5i). Through a set of preliminary numerical simulations, it was determined that the most important design factor is the ridge depth to channel height ratio. A sufficient depth is necessary to generate strong secondary flows capable of imparting a significant momentum to the main flow stream. The results presented here are for a depth to height ratio of one. Fig. 5i provides details of the design implemented in the numerical simulation. In Fig. 5ii, two pathlines in the solution microfilm are traced to illustrate the generation of transverse currents within the flow stream.

Fig. 6i shows a 3D view of the concentration contours depicting the impact of vortices on the concentration field. The numerical simulation presented in this section is conducted at a solution pressure of 30 kPa, a vapor pressure of 10 kPa, an inlet concentration of 52%, and a wall temperature of 103 °C. To better illustrate the process (i.e. the replenishment of the concentrated solution at the membrane–solution interface with the water-rich solution), the concentration contours at different cross sections are provided in

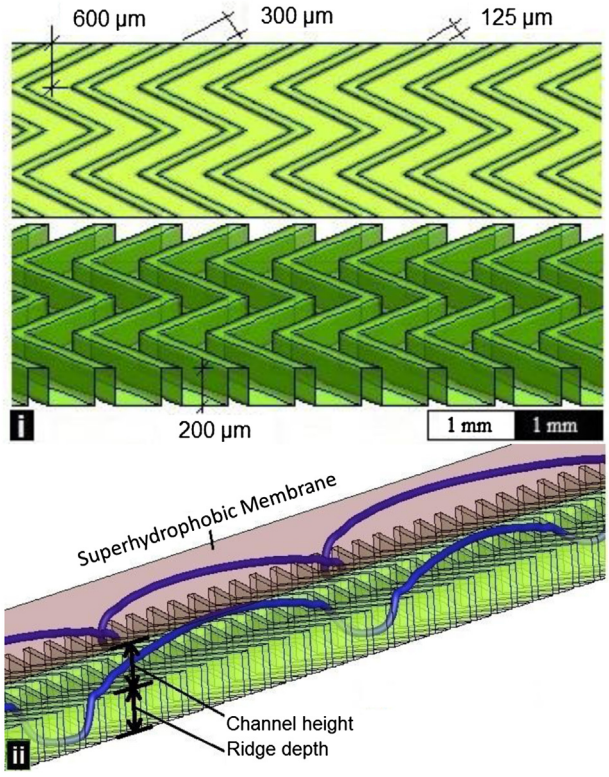

Fig. 5. (i) Staggered herringbone structures (i.e. micro-ridges) on the flow channel bottom wall (ii) two example pathlines in the solution flow.

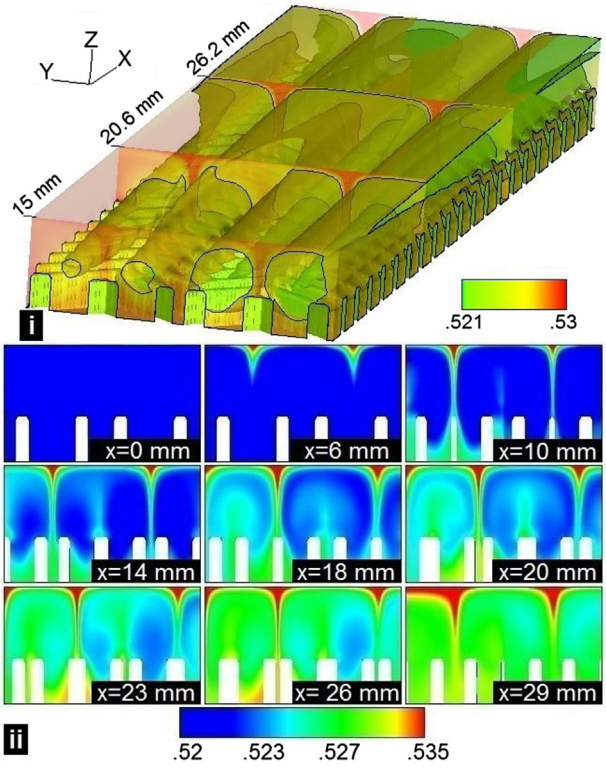

Fig. 6. (i) A 3D view of concentration contours (ii) LiBr concentration contours at different cross sections between $x = 0$–29 mm.

Fig. 6ii. The cross sections are chosen between $x = 0$ mm and $x = 29$ mm. At $x = 0$ mm, the bulk solution concentration is 52%. As the solution flows along the microchannel, the vortices bring the concentrated solution near the membrane down (cf. $x = 6$–14 mm). That volume of the solution is replaced with the water-rich solution brought up from the bottom of the flow channel (cf. $x = 18$–29 mm). The bulk concentration reached approximately 53.5% at $x = 29$ mm.

The concentration contours at $y = 1.32$ mm cross-section are shown in Fig. 7. A comparison of the results with those of the Base Case (cf. Fig. 4) clearly shows that the introduction of micro-ridges on the channel surface substantially modifies the concentration distribution. The transverse currents continuously interrupt the boundary layer growth and result in a uniform concentration distribution at each cross-section (compare Figs. 4 and 7). It is important to note that although the mass transfer mechanism within the bulk flow has changed from diffusion to convection, the desorption process at the membrane–solution interface is still diffusion limited.

Variations of important parameters in the solution flow are plotted in Fig. 8. At the desorber inlet, since the solution water vapor pressure is significantly lower than the external vapor

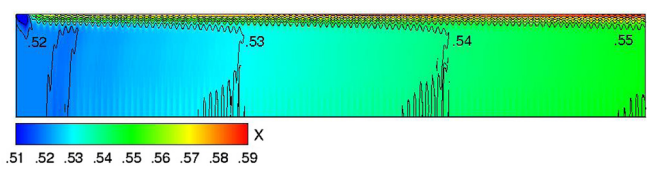

Fig. 7. LiBr solution concentration contours within a 200-micron-thick and 89-mm-long flow channel incorporating micro-ridges on the flow channel bottom wall.

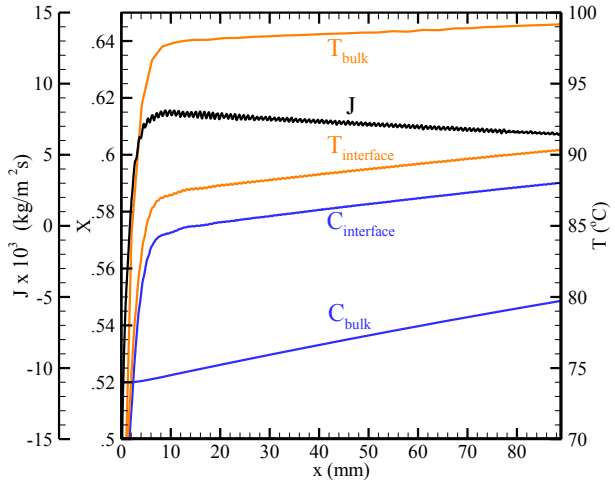

Fig. 8. Variations of concentration (C), desorption rate (J), and temperature (T) along the flow channel.

pressure, vapor is absorbed into the solution (i.e. a negative desorption rate). This phenomenon results in a significant reduction in the interface concentration. But, the high heat transfer coefficient associated with the microchannel flow results in rapid heating of the solution flow shortly after it enters the desorber. As a result, the solution water vapor pressure exceeds the external vapor pressure (i.e. 10 kPa), and the desorption process begins. As the water vapor desorbs from the solution, the interface and the bulk solution concentrations increase along the flow direction. The desorption rate gradually declines as the overall concentration of the solution increases along the flow channel. The average desorption rate from the solution in this case is approximately 0.0068 kg/m^2 s, which is about 1.7 times greater than that of the Base Case and 1.3 times higher than that of boiling at the same surface temperature (see Fig. 2 for a comparison of the results).

5. Conclusion

It is shown that the water desorption rate from a LiBr-water solution flow, when mechanically constrained by a porous membrane, could be significantly enhanced through the manipulation of the flow thermohydraulic characteristics. The key limitation in the desorption process is the slow diffusion of the water molecules through the LiBr solution. To overcome this limitation, surface-induced vortices were introduced to continuously replenish the concentrated solution at the membrane–solution interface with water-rich solution. The process effectively changes the mass transport mechanism within much of the solution flow, from molecular diffusion to convection. As a result, the desorption rate increased by a factor of 1.7 compared to that of direct diffusion, and by a factor of 1.3 compared to that of boiling.

Acknowledgements

The presented study was supported by a Grant from the Advanced Research Projects Agency-Energy (ARPA-E) under contract DE-AR0000133.

References

[1] W.W.S. Charters, V.R. Megler, W.D. Chen, Y.F. Wang, Atmospheric and subatmospheric boiling of H_2O and LiBr/H_2O solutions, Int. J. Refrig. 5 (1982) 107–114.
[2] C.C. Lee, Y.K. Chuah, D.C. Lu, H.Y. Chao, Experimental investigation of pool boiling of lithium bromide solution on a vertical tube under subatmospheric pressures, Int. Commun. Heat Mass Transfer 18 (1991) 309–320.
[3] H.K. Varma, R.K. Mehrotra, K.N. Agrawal, U.P. Roorkee, S. Singh, Heat transfer during pool boiling of LiBr–water solutions at subatmospheric pressures, Int. Commun. Heat Mass Transfer 21 (1994) 539–548.
[4] A. Matsuda, K. Hada, T. Kawamura, A vertical falling film type of absorber and generator for lithium bromide aqueous solutions, Trans. Jpn. Assoc. Refrig. 7 (1990) 47–56.
[5] A. Matsuda, T. Kawamura, K. Hada, Evaporation for lithium bromide aqueous solution in a vertical falling film type of generator under reduced pressure, Trans. Jpn. Assoc. Refrig. 7 (1990) 35–45.
[6] D. Kim, M. Kim, Heat transfer enhancement characteristics for falling-film evaporation on horizontal enhanced tubes with aqueous LiBr solution, J. Enhanced Heat Transfer 6 (1999) 61–69.
[7] T. Fujita, Falling liquid films in absorption machines, Int. J. Refrig. 16 (1993) 282–294.
[8] H. Yoshitomi, O. Tajima, T. Takeuchi, H. Hara, Refrigeration 56 (1981) 271.
[9] V.E. Nakoryakov, N.I. Grigor'eva, S.I. Lezhnin, L.V. Potaturkina, Combined heat and mass transfer in film absorption and bubble desorption, Heat Transfer Res. 29 (1998) 333–338.
[10] D. Yu, J. Chung, S. Moghaddam, Parametric study of water vapor absorption into a constrained thin film of lithium bromide solution, Int. J. Heat Mass Transfer 55 (2012) 5687–5695.
[11] R.N. Isfahani, S. Moghaddam, Absorption characteristics of lithium bromide (LiBr) solution constrained by superhydrophobic nanofibrous structures, Int. J. Heat Mass Transfer 63 (2013) 82–90.
[12] R. Nasr Isfahani, K. Sampath, S. Moghaddam, Nanofibrous membrane-based absorption refrigeration system, Int. J. Refrig. 36 (2013) 2297–2307.
[13] R.N. Isfahani, A. Fazeli, S. Bigham, S. Moghaddam, Physics of lithium bromide (LiBr) solution dewatering through vapor venting membranes, Int. J. Multiphase Flow 58 (2014) 27–38.
[14] S. Bigham, D. Yu, D. Chugh, S. Moghaddam, Moving beyond the limits of mass transport in liquid absorbent microfilms through the implementation of surface-induced vortices, Energy (Dec. 2013).
[15] J.D. Thorud, J.A. Liburdy, D.V. Pence, Microchannel membrane separation applied to confined thin film desorption, Exp. Therm. Fluid Sci. 30 (2006) 713–723.
[16] A.P. Sudarsan, V.M. Ugaz, Multivortex micromixing, Proc. Natl. Acad. Sci. U. S. A. 103 (2006) 7228–7233.
[17] J.M. Ottino, S. Wiggins, Designing optimal micromixers, Science 305 (2004) 485–486.
[18] C. Xi, D.L. Marks, D.S. Parikh, L. Raskin, S.A. Boppart, Structural and functional imaging of 3D microfluidic mixers using optical coherence tomography, Proc. Natl. Acad. Sci. U. S. A. 101 (2004) 7516–7521.
[19] A.D. Stroock, S.K.W. Dertinger, A. Ajdari, I. Mezic, H.A. Stone, G.M. Whitesides, Chaotic mixer for microchannels, Science 295 (2002) 647–651.
[20] E.A. Mason, A.P. Malinauskas, Gas transport in Porous Media: the Dusty-gas Model, Elsevier Scientific Pub, New York, 1983.
[21] S. Jeong, S. Garimella, Falling-film and droplet mode heat and mass transfer in a horizontal tube LiBr/water absorber, Int. J. Heat Mass Transfer 45 (2002) 1445–1458.
[22] L.A. McNeely, Thermodynamic properties of aqueous solutions of lithium bromide, ASHRAE Trans. 85 (1979) 413–434.
[23] D. Yu, A.J.C. Ladd, A numerical simulation method for dissolution in porous and fractured media, J. Comput Phys. 229 (2010) 6450–6465.
[24] X. He, L. Luo, A priori derivation of the lattice Boltzmann equation, Phys. Rev. E 55 (1997) 6333–6336.